Title:

Activating mutations in *ESR1* contribute to an immunosuppressive breast tumor microenvironment by dampening cytokine secretion

Authors:

Yu Gu [1, 2], Dongmei Zuo [1], Qixin Hu [1, 3], Virginie Sanguin-Gendreau [1], Alain Pacis [4], Marie-Christine Guiot [5], Alexander Chih-Chieh Chang [6, 7], Tarek Taifour [1, 8], Chen Ling [1], Adrian V Lee [6, 7], Steffi Oesterreich [6, 7], and William J. Muller [1, 2, 9]

Supplemental Material

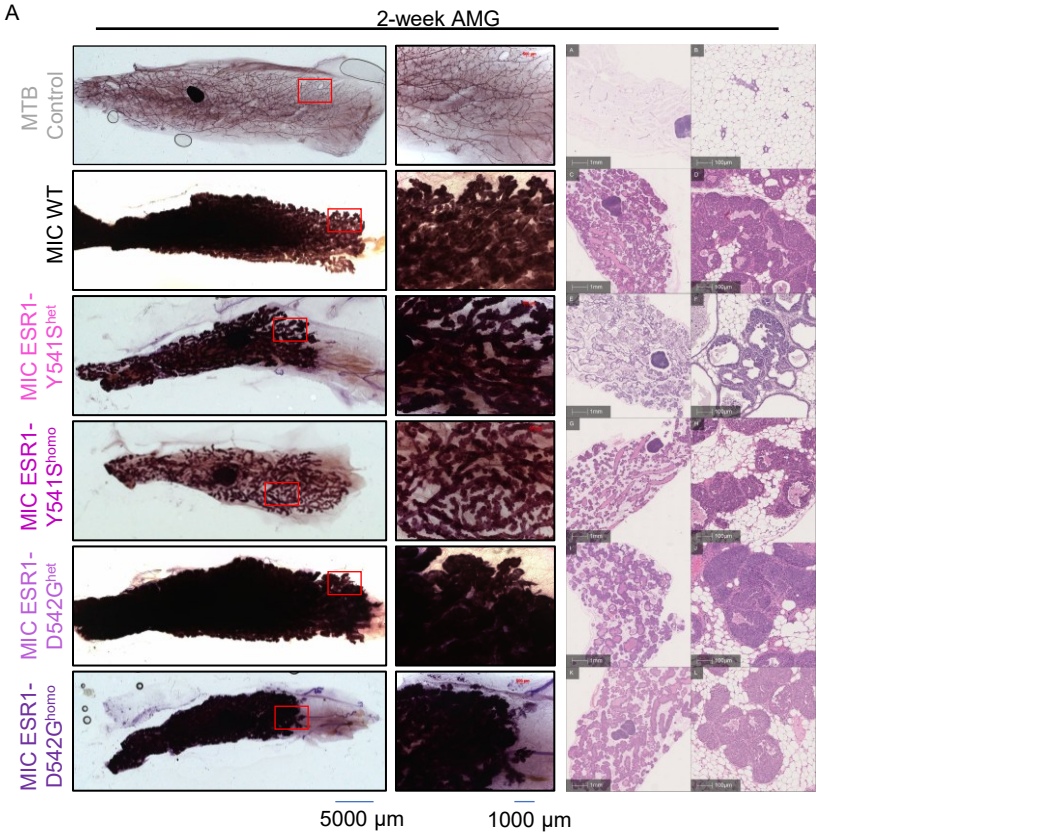

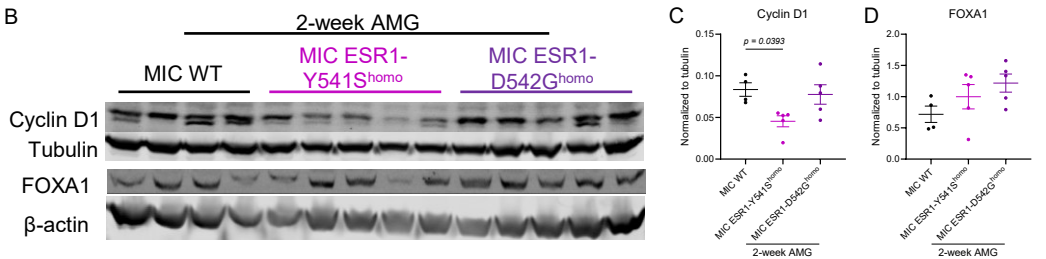

Supplemental Figure 1. Characterization of mammary glands 2 weeks post-DOX induction in MIC WT and ESR1^{mut} mice. A. Representative images of whole mount analysis and H&E images of mammary gland (AMG) epithelial transformation (tumour initiation) after 2 weeks post-DOX induction in MTB control (n = 4), MIC WT (n = 5), MIC ESR1-Y541S^{het} (n = 6), MIC ESR1-Y541S^{homo} (n = 7), MIC ESR1-D542G^{het} (n = 7), and MIC ESR1-D542G^{homo} (n = 6) mice. B. Immunoblot for cyclin D1 and FOXA1 with their respective loading control (Tubulin and β-actin) on 2 weeks post-DOX induction AMG lysates of MIC WT, MIC ESR1-Y541S^{homo}, and MIC ESR1-D542G^{homo} mice. C-D. Quantification of immunoblot for cyclin D1 and FOXA1 normalized to their respective loading control, respectively. Scale bars are as indicated on each image. Mean ± SEM for data calculated using one-way ANOVA with Tukey's multiple comparisons test.

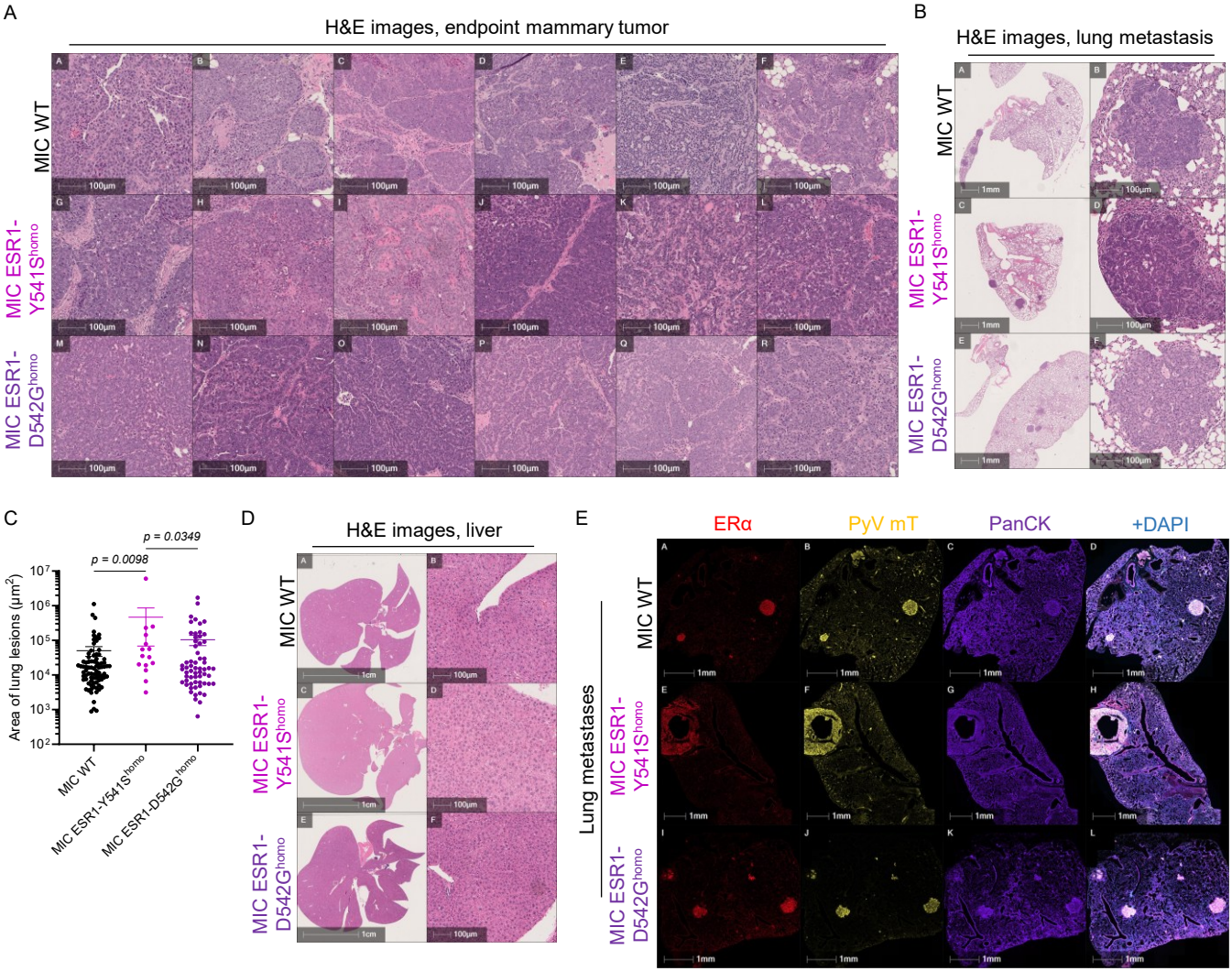

Supplemental Figure 2. Representative H&E images of endpoint mammary tumors, lungs, and liver in MIC WT and ESR1^{mut} mice. A. Representative H&E images of endpoint mammary tumors of MIC WT, MIC ESR1-Y541S^{homo}, and MIC ESR1-D542G^{homo} mice. B. Representative H&E images of lungs collected at endpoint of mammary tumor mass of MIC WT (n = 10), MIC ESR1-Y541S^{homo} (n = 6), and MIC ESR1-D542G^{homo} (n = 10) mice. C. Quantification of area of lung metastatic lesions. D. Representative H&E images of livers collected at endpoint of mammary tumor of MIC WT (n = 10), MIC ESR1-Y541S^{homo} (n = 6), and MIC ESR1-D542G^{homo} (n = 10) mice. E. Fluorescent IHC for ERα, PyV mT, PanCK, and DAPI on lung metastases of MIC WT, MIC ESR1-Y541S^{homo}, and MIC ESR1-D542G^{homo} mice. Scale bars are as indicated on each image. Mean ± SEM for data calculated using one-way ANOVA with Tukey's multiple comparisons test.

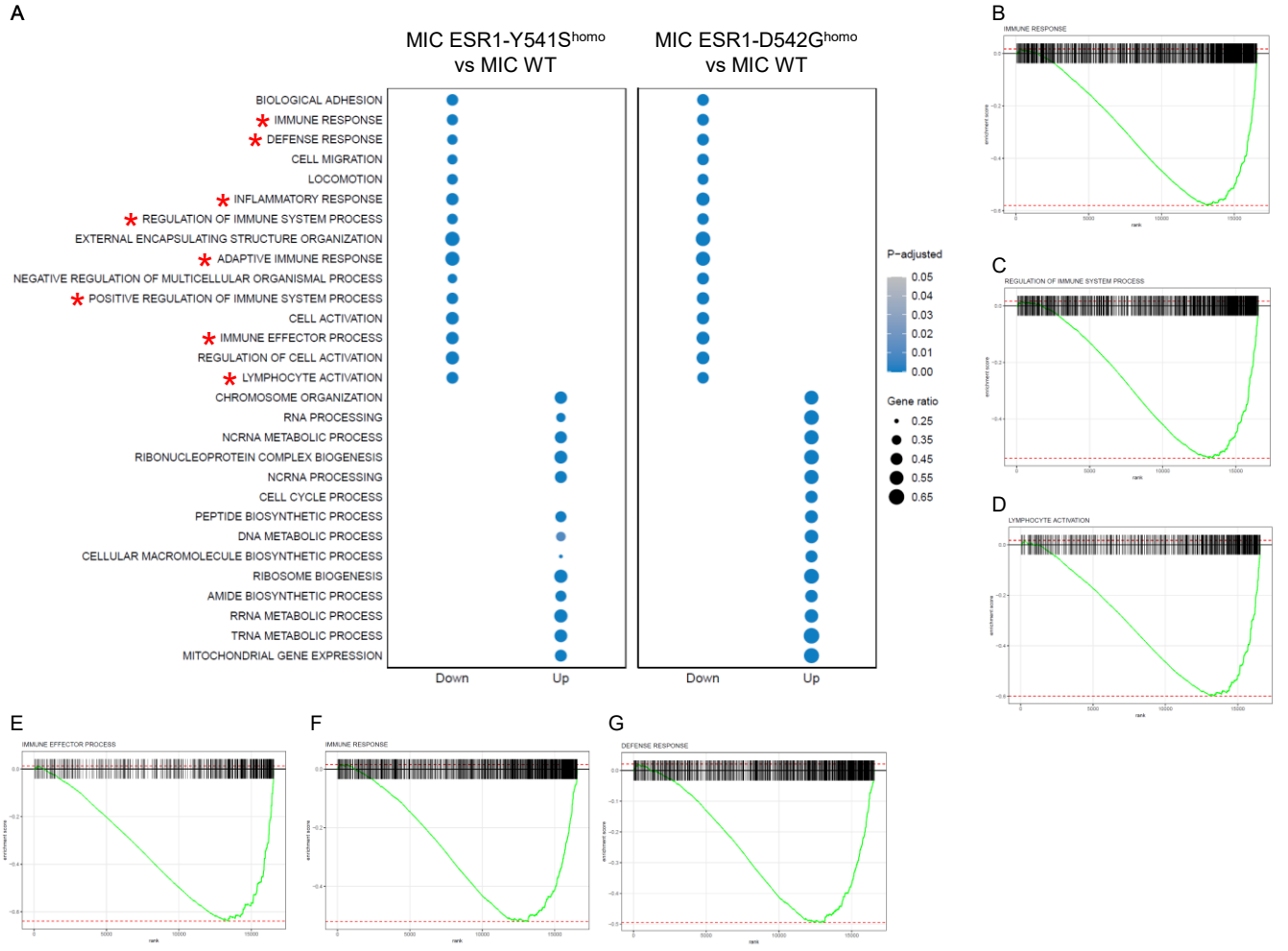

Supplemental Figure 3. GSEA analysis on MIC WT and MIC ESR1-Y541S^{homo} or MIC ESR1-D542G^{homo} endpoint mammary tumor RNA sequencing. A. Dot plots representing the changes in GSEA hallmark pathways between MIC ESR1-Y541S^{homo} tumors versus MIC WT tumors and MIC ESR1-D542G^{homo} tumors versus MIC WT tumors with stars delineating immune-related pathways. B-E. Immune response, regulation of immune system process, lymphocyte activation, and immune effector process are negatively regulated in MIC ESR1-Y541S^{homo} tumors versus MIC WT tumors, respectively. F-G. Immune response and defense response are negatively regulated in MIC ESR1-D542G^{homo} tumors versus MIC WT tumors, respectively.

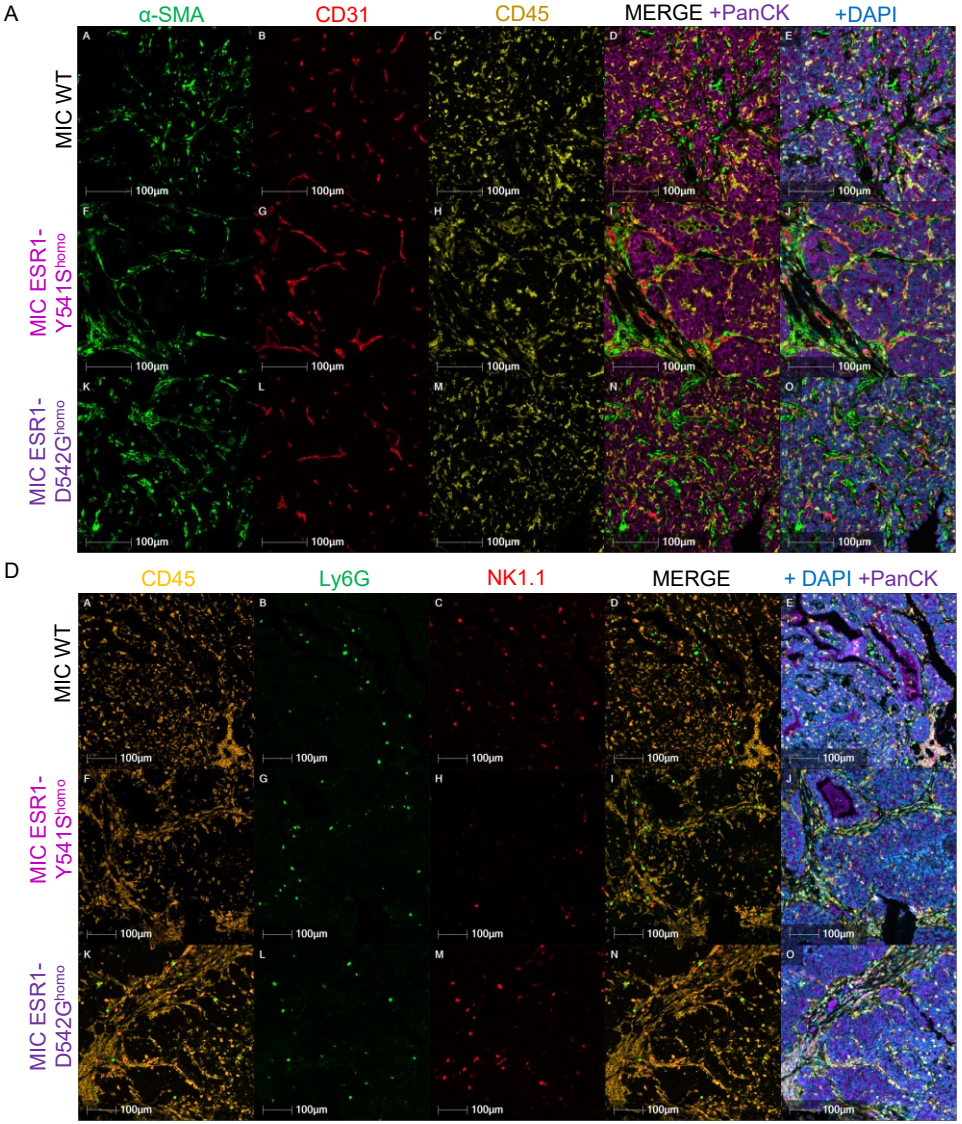

Supplemental Figure 4. Characterization of total immune cells, endothelial cells, neutrophils, and NK cells in endpoint mammary tumors. A. Fluorescent IHC for α-SMA, CD31, CD45, PanCK, and DAPI on endpoint mammary tumors of MIC WT, MIC ESR1-Y541S^{homo}, and MIC ESR1-D542G^{homo} mice. B-C. Quantification of α-SMA+ cells and CD31+ cells, respectively. D. Fluorescent IHC for CD45, Ly6G, NK1.1, PanCK, and DAPI on endpoint mammary tumors of MIC WT, MIC ESR1-Y541S^{homo}, and MIC ESR1-D542G^{homo} mice. E-G. Quantification of CD45+ cells, Ly6G+ CD45+ cells, and NK1.1+ CD45+ cells, respectively. Scale bars are as indicated on each image. Mean ± SEM for data calculated using one-way ANOVA with Tukey's multiple comparisons test.

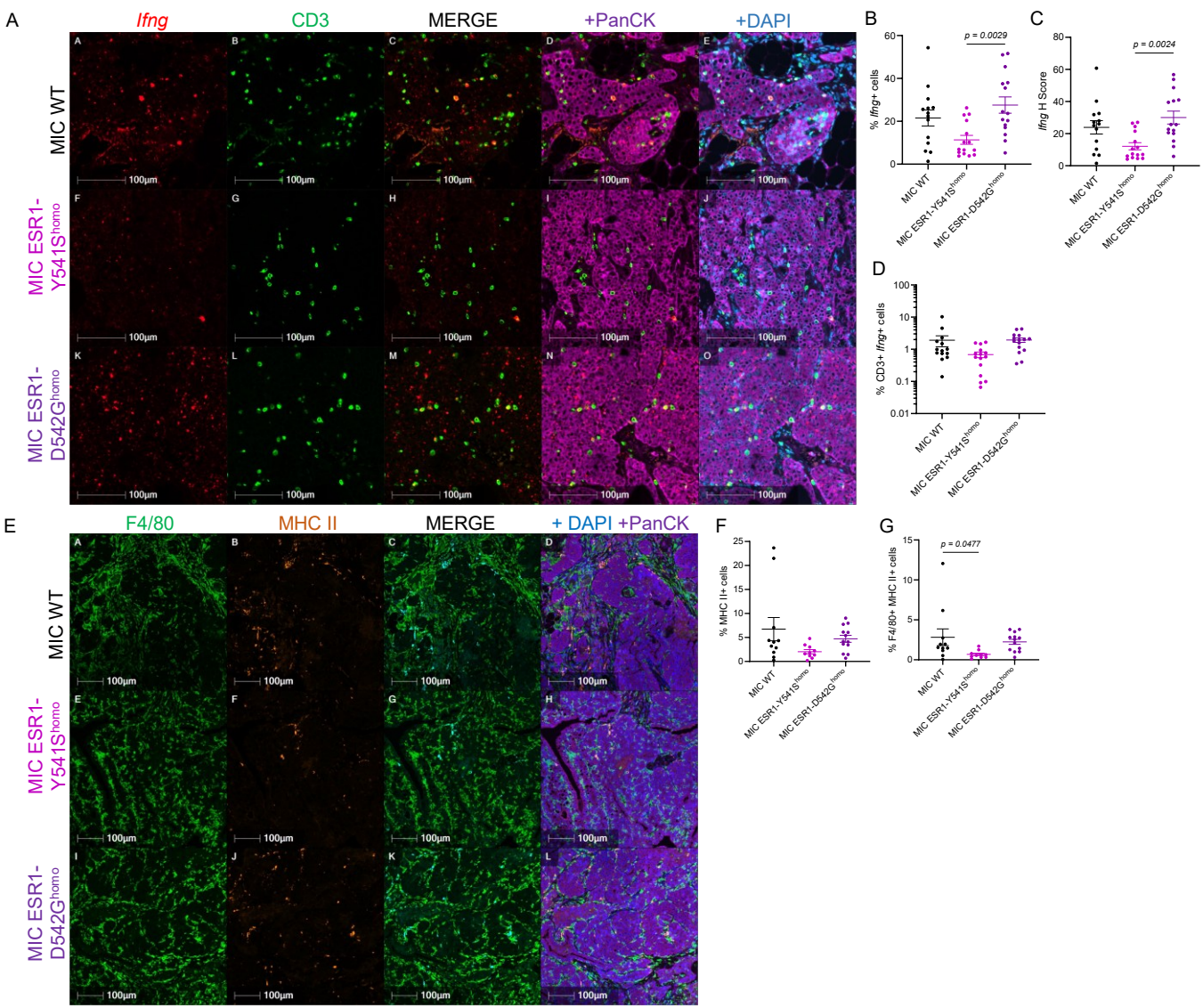

Supplemental Figure 5. MIC ESR1-Y541S^{homo} endpoint mammary tumors have decreased T cell and macrophage activities. A. RNA FISH for mouse *Ifng* and fluorescent IHC for CD3, PanCK, and DAPI on endpoint mammary tumors of MIC WT, MIC ESR1-Y541S^{homo}, and MIC ESR1-D542G^{homo} mice. B-D. Quantification of *Ifng*+ cells, *Ifng* H Score, and CD3+ *Ifng*+ cells, respectively. E. Fluorescent IHC for F4/80, MHC II, PanCK, and DAPI on endpoint mammary tumors of MIC WT, MIC ESR1-Y541S^{homo}, and MIC ESR1-D542G^{homo} mice. F-G. Quantification of MHC II+ cells and F4/80+ MHC II+ cells, respectively. Scale bars are as indicated on each image. Mean ± SEM for data calculated using one-way ANOVA with Tukey's multiple comparisons test.

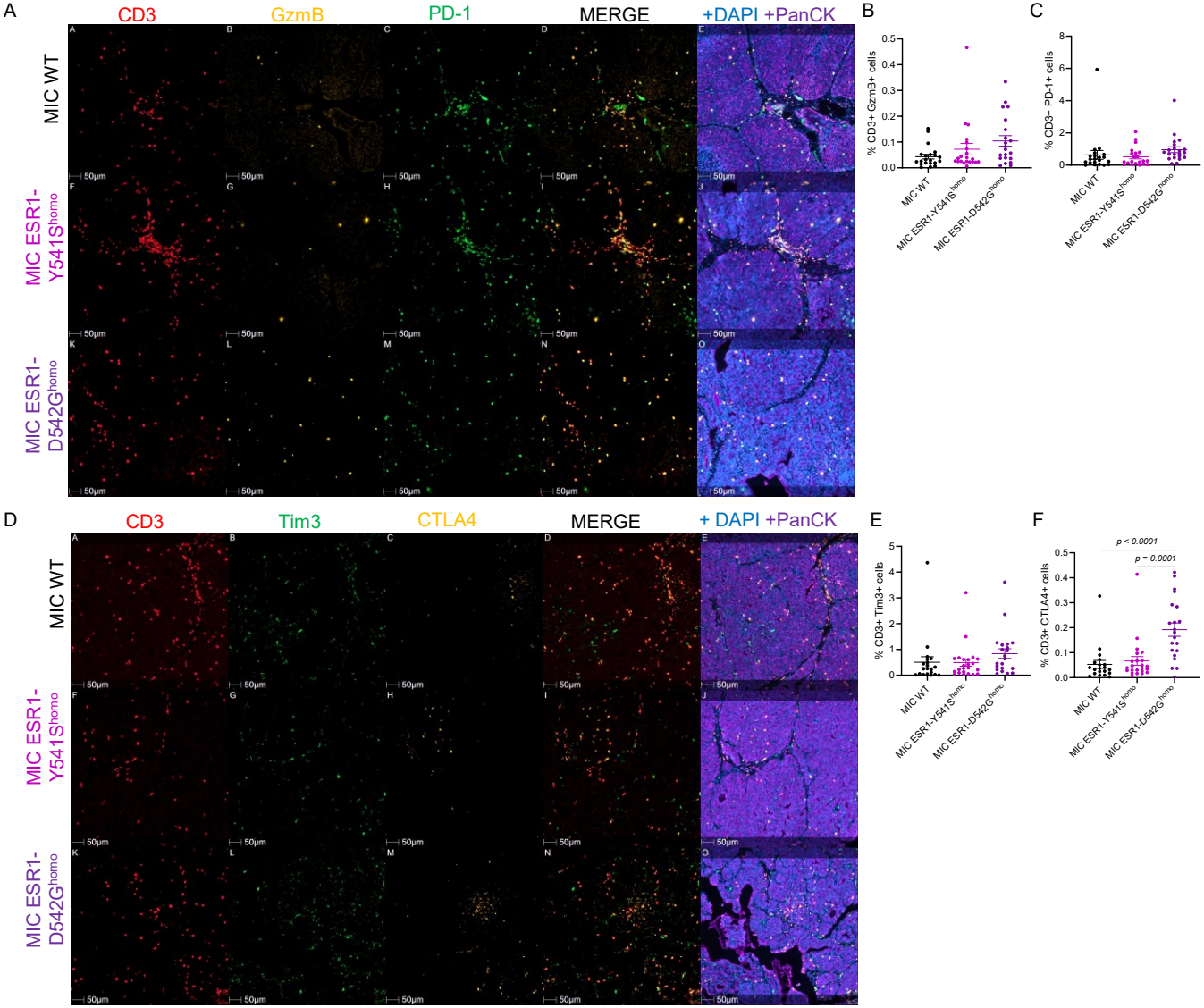

Supplemental Figure 6. Characterization of T cell activation and exhaustion in endpoint mammary tumors. A. Fluorescent IHC for CD3, granzyme B (GzmB), PD-1, PanCK, and DAPI on endpoint mammary tumors of MIC WT, MIC ESR1-Y541S^{homo}, and MIC ESR1-D542G^{homo} mice. B-C. Quantification of CD3+ GzmB+ cells and CD3+ PD-1+ cells, respectively. D. Fluorescent IHC for CD3, Tim3, CTLA4, PanCK, and DAPI on endpoint mammary tumors of MIC WT, MIC ESR1-Y541S^{homo}, and MIC ESR1-D542G^{homo} mice. E-F. Quantification of CD3+ Tim3+ cells and CD3+ CTLA4+ cells, respectively. Scale bars are as indicated on each image. Mean ± SEM for data calculated using one-way ANOVA with Tukey's multiple comparisons test.

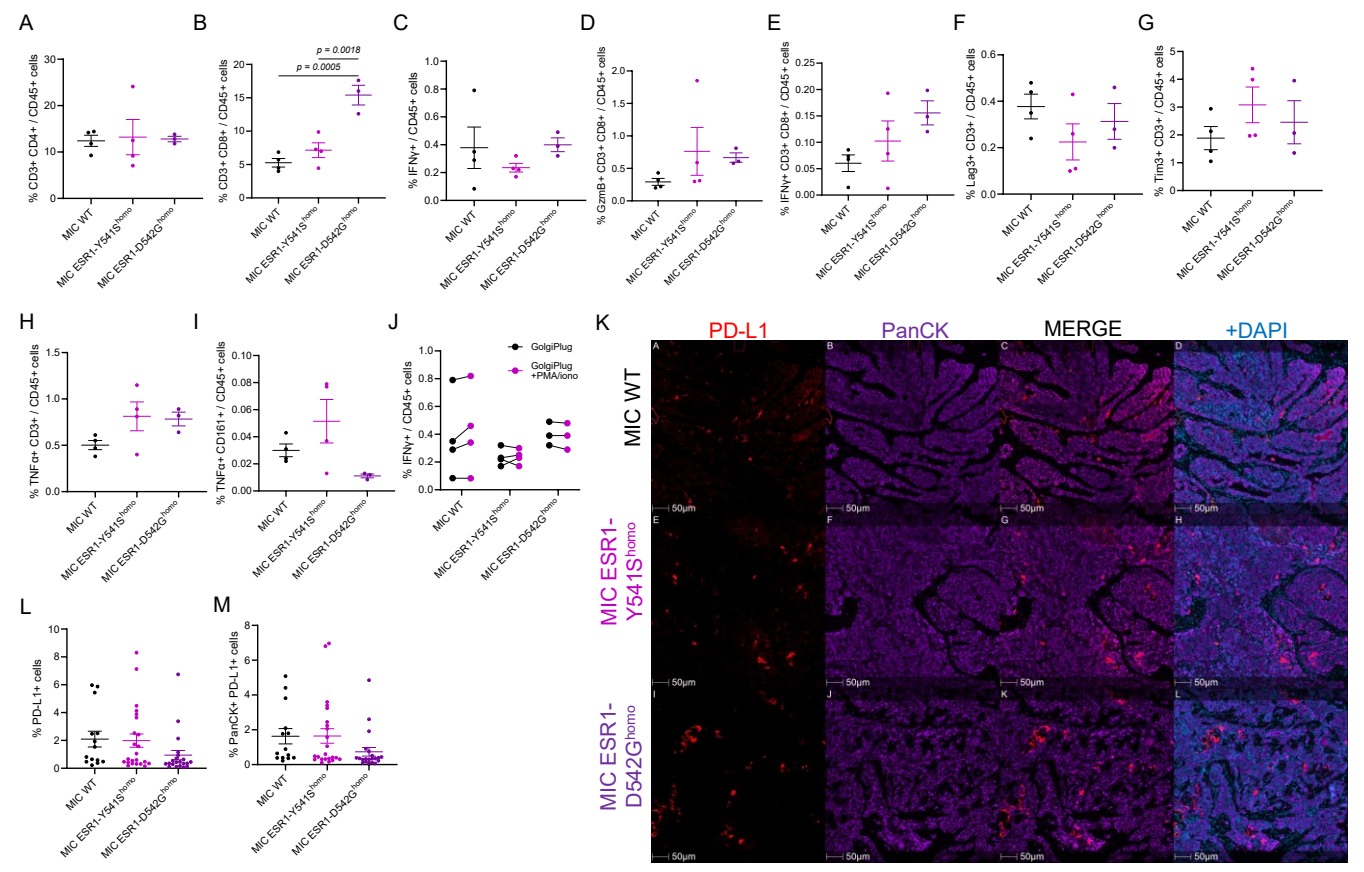

Supplemental Figure 7. Characterization of functional states of immune cells by flow cytometry in endpoint mammary tumors. A-I. Quantification of CD3+ CD4+ cells, CD3+ CD8+ cells, IFNγ+ cells, GzmB+ CD3+ CD8+ cells, IFNγ+ CD3+ CD8+ cells, Lag3+ CD3+ cells, Tim3+ CD3+ cells, TNFα+ CD3+ cells, and TNFα+ CD161+ cells out of total CD45+ cells by flow cytometry, respectively. J. IFNγ+ cells out of total CD45+ cells with or without PMA/ionomycin stimulation in endpoint mammary tumors of MIC WT, MIC ESR1-Y541S^{homo}, and MIC ESR1-D542G^{homo} mice by flow cytometry. K. Fluorescent IHC for PD-L1, PanCK, and DAPI on endpoint mammary tumors of MIC WT, MIC ESR1-Y541S^{homo}, and MIC ESR1-D542G^{homo} mice. L-M. Quantification of PD-L1+ cells and PanCK+ PD-L1+ cells, respectively. Scale bars are as indicated on each image. Mean ± SEM for data calculated using one-way ANOVA with Tukey's multiple comparisons test.

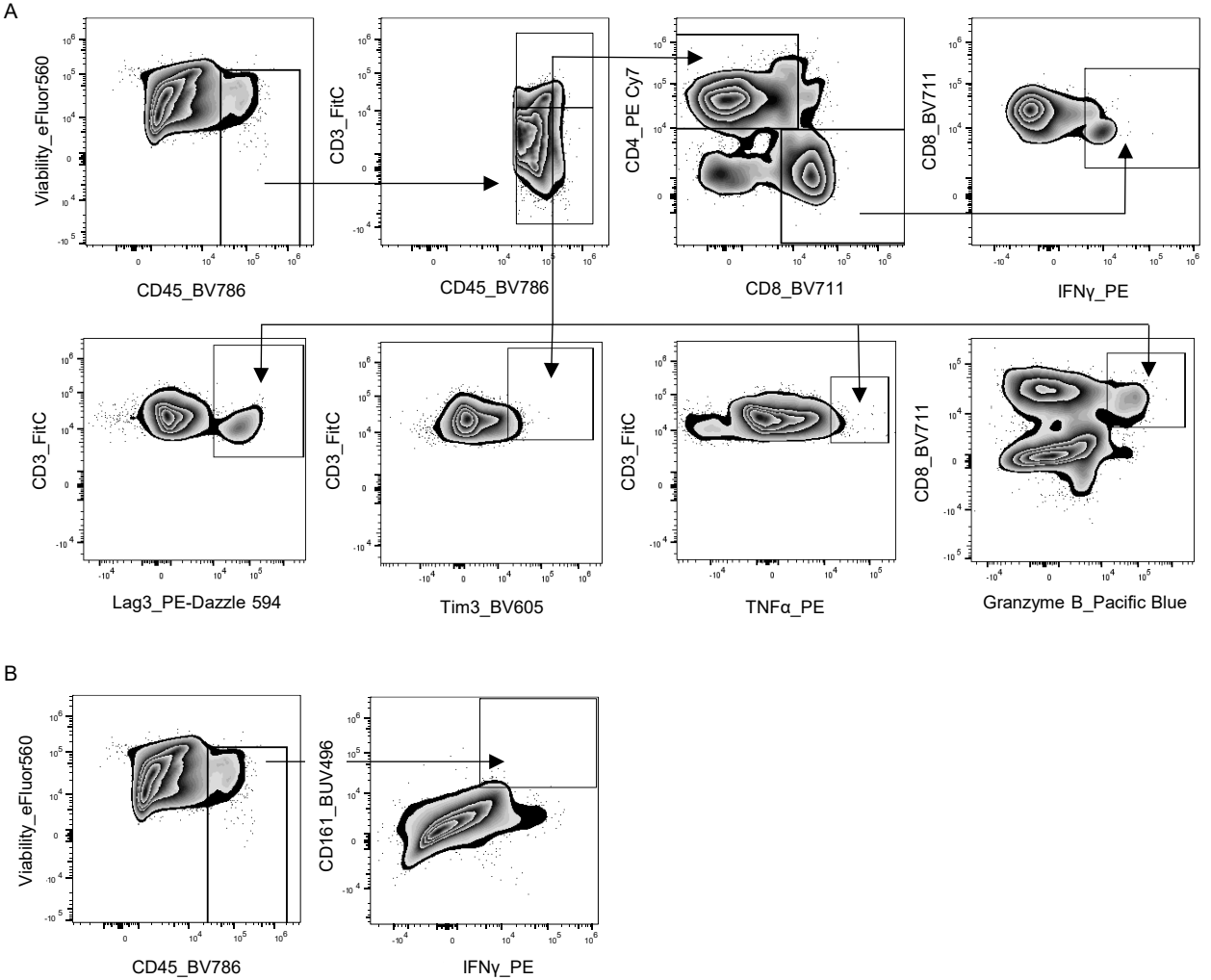

Supplemental Figure 8. Flow cytometry gating for immune cells and their functional markers on endpoint mammary tumors. A. Flow cytometry gating strategy for viable CD45+ immune cells, then CD3+ total T cells, then CD4+ T cells and CD8+ T cells. CD8+ T cells are gated for IFNγ+. CD3+ T cells are gated for Lag3+, Tim3+, TNFα+, and CD8+ granzyme B+ cells. B. Representative flow cytometry gating strategy for viable CD45+ immune cells then IFNγ+ CD161+ NK cells. A-B depict a representative sample for endpoint mammary tumors of MIC WT (n = 4), MIC ESR1-Y541S^{homo} (n = 4), and MIC ESR1-D542G^{homo} (n = 3) mice. Created on FlowJo.

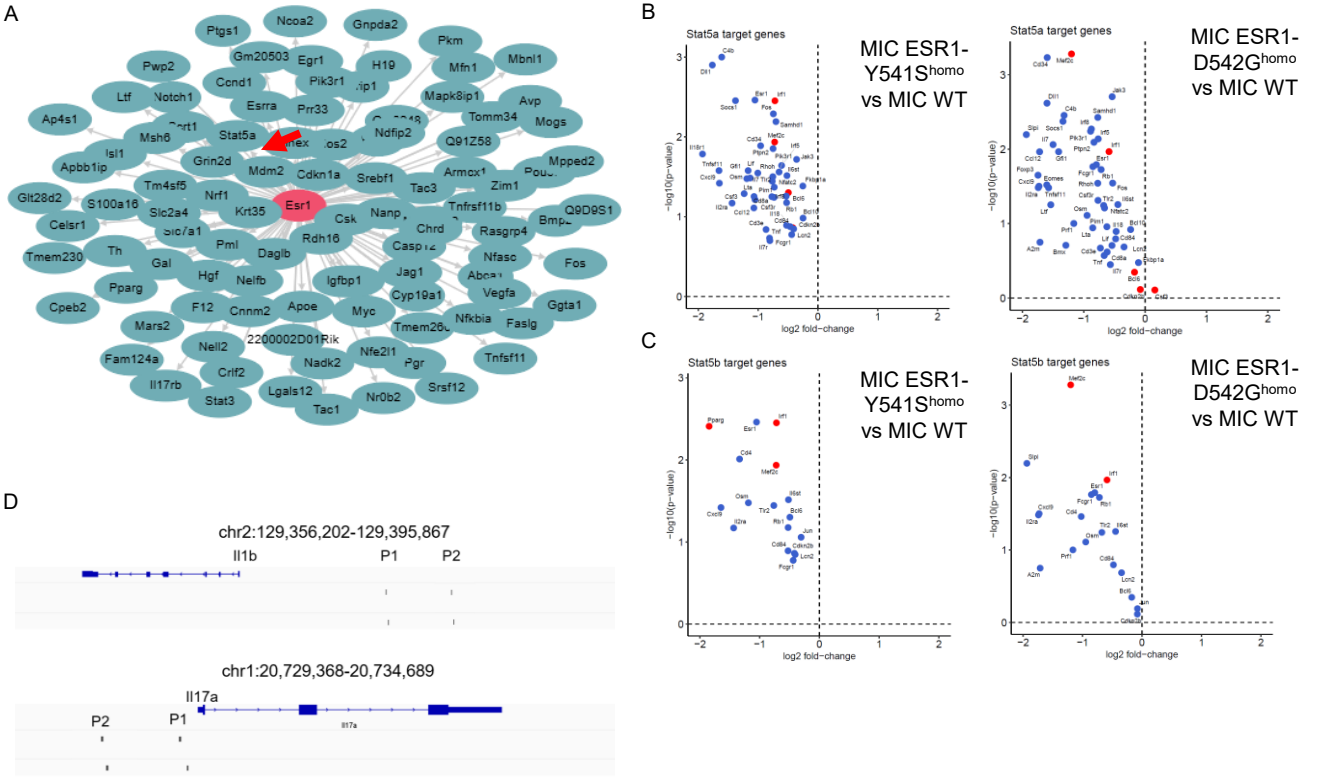

Supplemental Figure 9. Stat5 is a target of ERα and contributes to the decreased immune pathway activity in MIC ESR1^{mut} tumors. A. Transcription factor network for ERα (*Esr1*) indicating Stat5 as a transcription target of ERα using tflink.net. B-C. Volcano plot depicting Stat5a and Stat5b transcription factor-target genes contributing to the downregulated immune-related pathways in MIC ESR1-Y541S^{homo} or MIC ESR1-D542G^{homo} vs MIC WT tumors, respectively. Blue color denotes that the target genes are deactivated and concordant to the known direction of *ESR1^{mut}*-target interaction. Red color denotes that the target genes are deactivated but discordant to the known direction of *ESR1^{mut}*-target interaction. D. ChIP-qPCR primer positions for *Il1b* and *Il17a* promoters shown on IGV for Figure 8J.

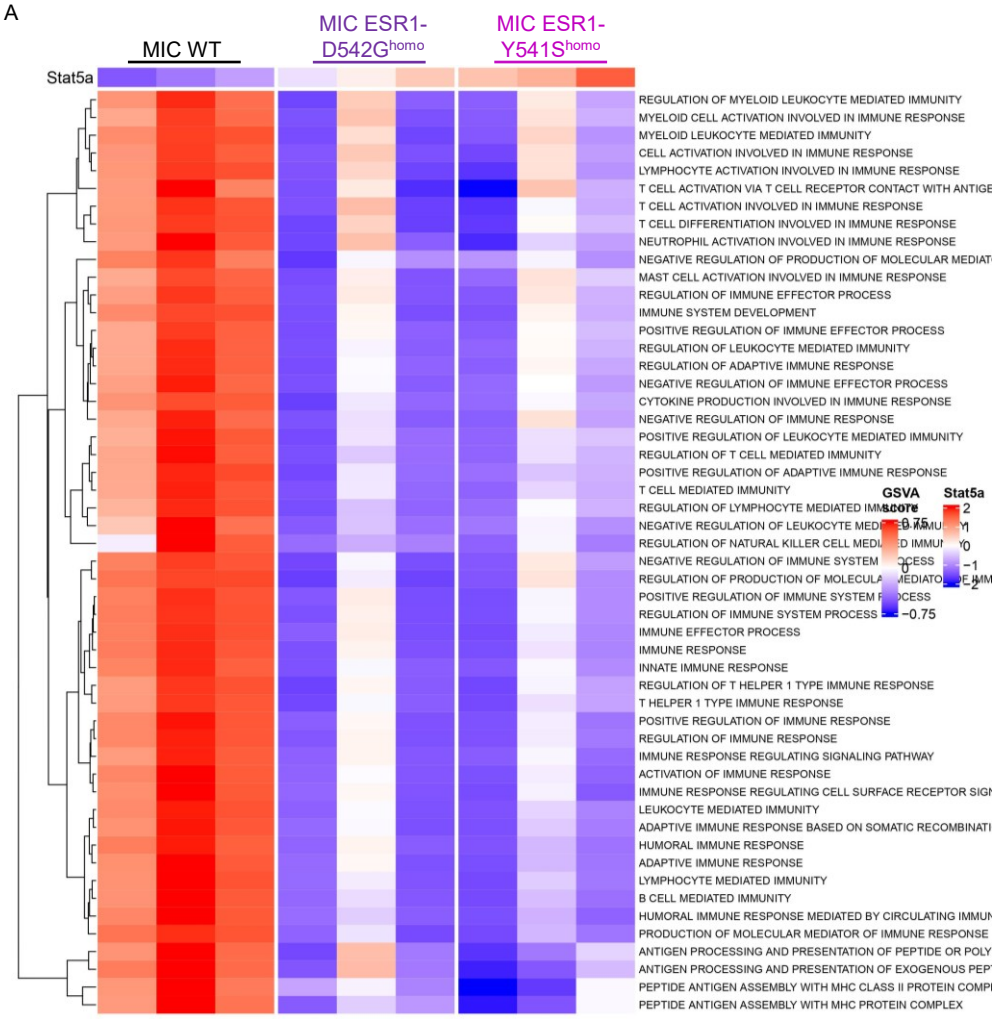

Supplemental Figure 10. High-Stat5a expression correlates with decreased immune pathway activity. A. Stat5a expression correlation map between MIC WT, MIC ESR1-Y541S^{homo}, and MIC ESR1-D542G^{homo} tumors and immune-related pathway activity from bulk RNA sequencing.

A

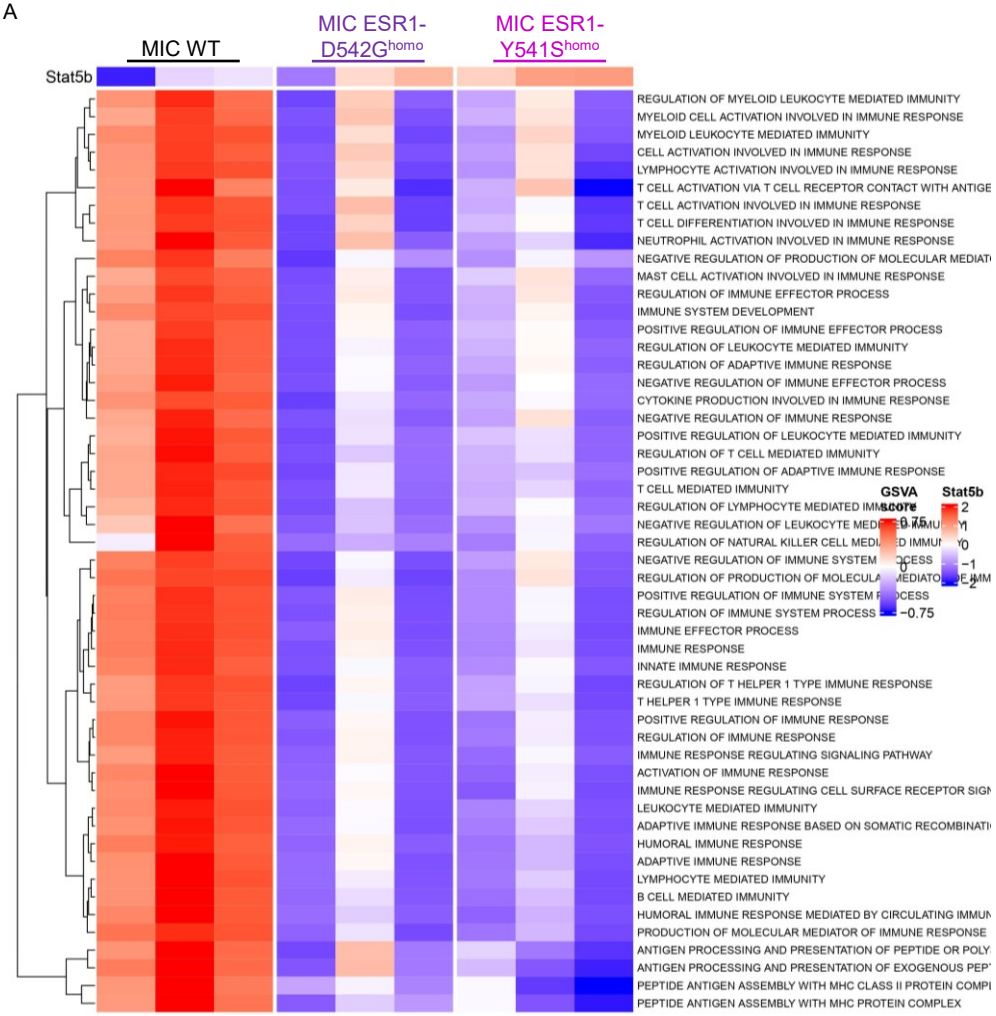

Supplemental Figure 11. High-Stat5b expression correlates with decreased immune pathway activity. A. Stat5b expression correlation map between MIC WT, MIC ESR1-Y541S^{homo}, and MIC ESR1-D542G^{homo} tumors and immune-related pathway activity from bulk RNA sequencing.

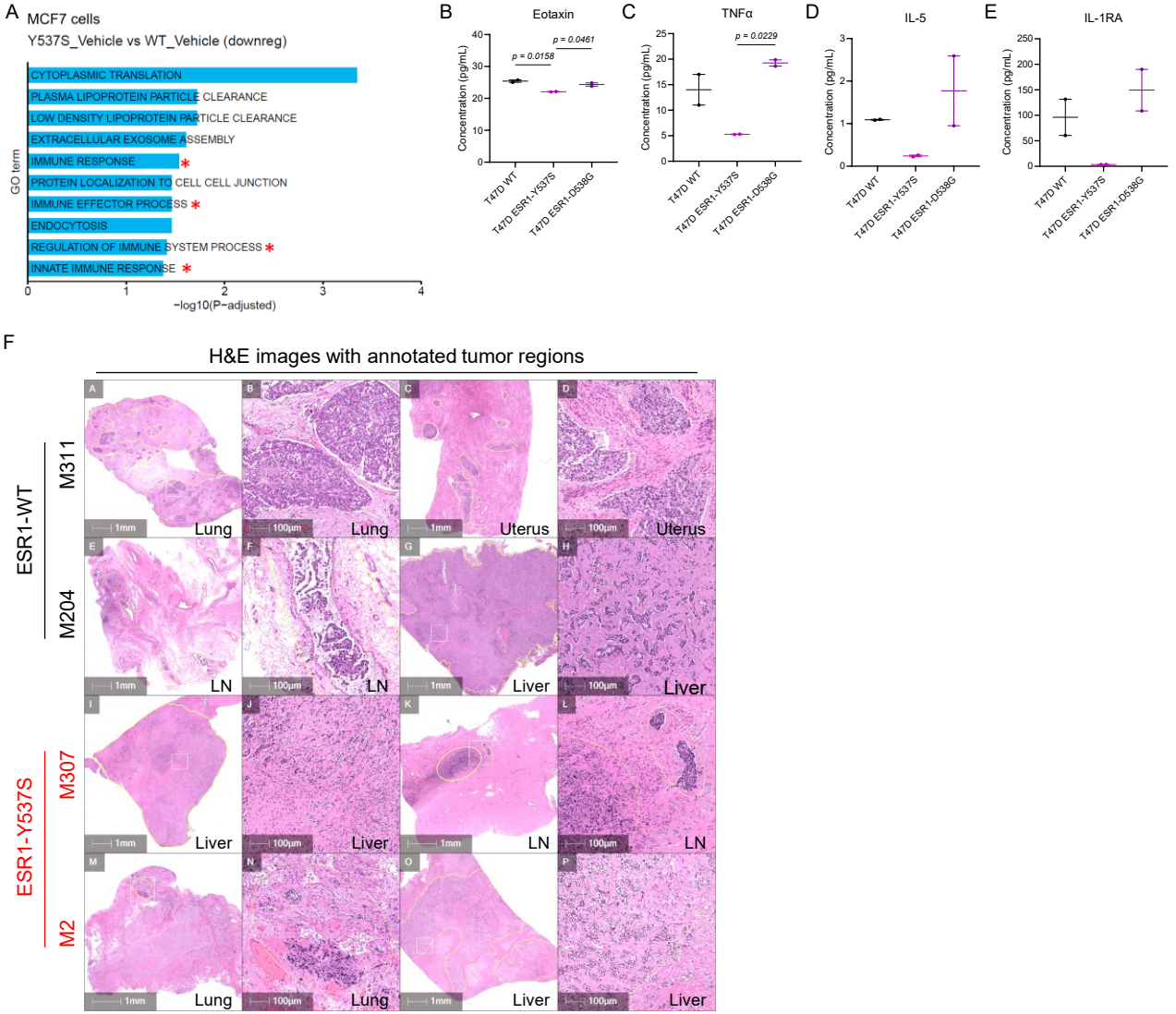

Supplemental Figure 12. *ESR1*^{Y537S} human breast cancer cell line and *ESR1*^{Y537S} metastatic breast cancer patient tumors analyses. A. Top Gene Ontology (GO) terms identified from downregulated DEG between MCF7 ESR1-WT and MCF7 ESR1-Y537S tumors from dataset GEO accession GSE266932, with stars delineating immune-related pathways. B-E. Quantification of observed concentrations of Eotaxin, TNFα, IL-5, and IL-1RA from cytokine multiplex assay on T47D WT, ESR1-Y537S, and ESR1-D538G human breast cancer cells, respectively. Each data point represents the mean of triplicate measurements. F. Representative H&E images of ESR1-WT and ESR1-Y537S patient metastases with annotations of pathological evaluation of tumor regions. Scale bars are as indicated on each image. Mean ± SEM for data calculated using one-way ANOVA with Tukey's multiple comparisons.

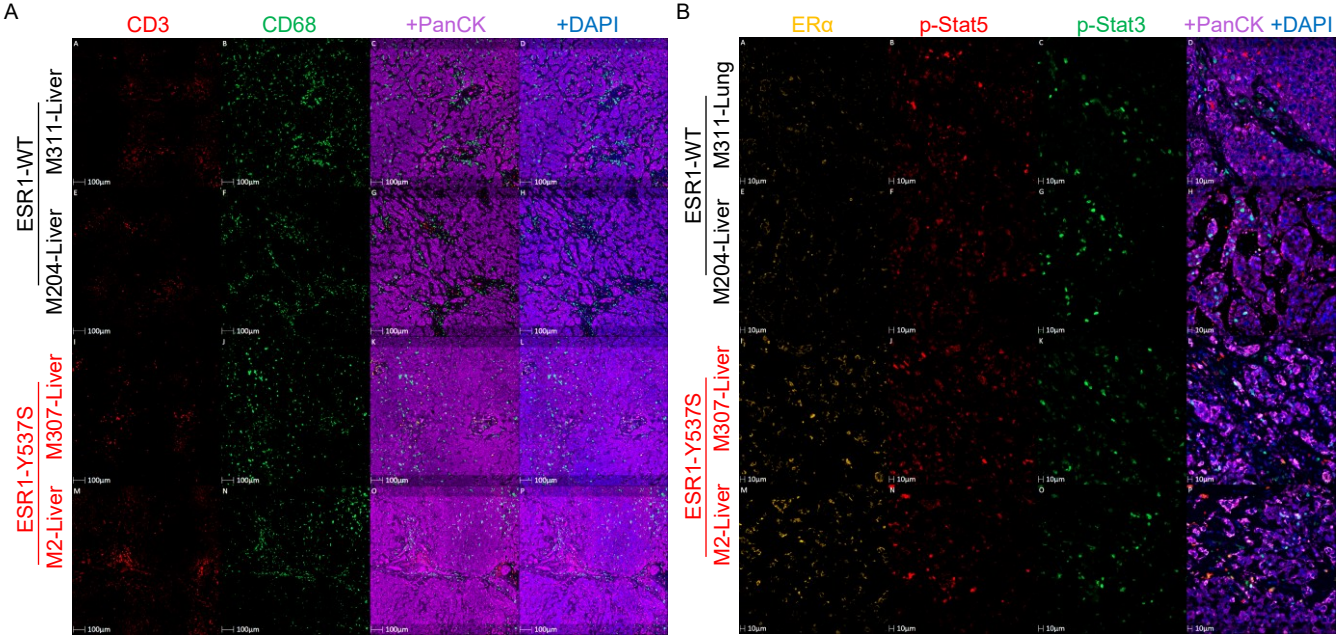

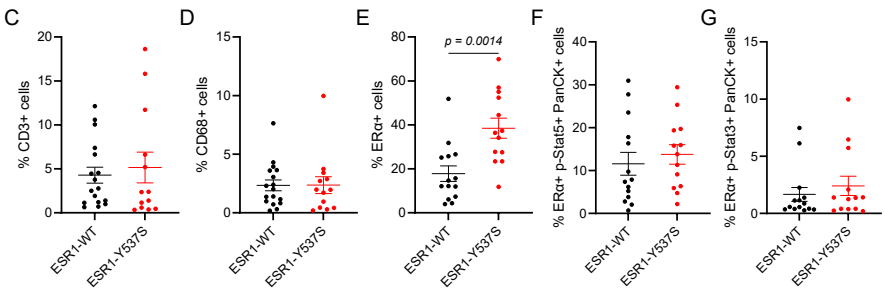

Supplemental Figure 13. *ESR1*^{Y537S} metastatic breast cancer patient tumors have comparable immune cell populations but elevated ERα levels. A. Fluorescent IHC for CD3, CD68, PanCK, and DAPI on ESR1-WT and ESR1-Y537S patient tumors. B. Fluorescent IHC for ERα, p-Stat5, p-Stat3, PanCK, and DAPI on ESR1-WT and ESR1-Y537S patient tumors. C-D. Quantification of CD3+ cells and CD68+ cells by ER mutation status, respectively. E-G. Quantification of ERα+ cells, ERα+ p-Stat5+ PanCK+ cells, and ERα+ p-Stat3+ PanCK+ cells by ER mutation status, respectively. Scale bars are as indicated on each image. Mean ± SEM for data calculated using two-tailed Student's t test.